Title

Mapping the mammalian ribosome quality control complex interactome using proximity labeling approaches

Journal

Molecular Biology of the Cell, 29(10)

ISSN

1059-1524

Authors

Zuzow, Nathan
Ghosh, Arit
Leonard, Marilyn
et al.

Publication Date

2018-05-15

DOI

10.1091/mbc.e17-12-0714

Peer reviewed

Mapping the mammalian ribosome quality control complex interactome using proximity labeling approaches

Nathan Zuzow, Arit Ghosh, Marilyn Leonard, Jeffrey Liao, Bing Yang, and Eric J. Bennett*
Section of Cell and Developmental Biology, Division of Biological Sciences, University of California, San Diego, La Jolla, CA 92093

ABSTRACT **Previous genetic and biochemical studies from *Saccharomyces cerevisiae* have identified a critical ribosome-associated quality control complex (RQC) that facilitates resolution of stalled ribosomal complexes. While components of the mammalian RQC have been examined in vitro, a systematic characterization of RQC protein interactions in mammalian cells has yet to be described. Here we utilize both proximity-labeling proteomic approaches, BioID and APEX, and traditional affinity-based strategies to both identify interacting proteins of mammalian RQC members and putative substrates for the RQC resident E3 ligase, Ltn1. Surprisingly, validation studies revealed that a subset of substrates are ubiquitylated by Ltn1 in a regulatory manner that does not result in subsequent substrate degradation. We demonstrate that Ltn1 catalyzes the regulatory ubiquitylation of ribosomal protein S6 kinase 1 and 2 (RPS6KA1, RPS6KA3). Further, loss of Ltn1 function results in hyperactivation of RSK1/2 signaling without impacting RSK1/2 protein turnover. These results suggest that Ltn1-mediated RSK1/2 ubiquitylation is inhibitory and establishes a new role for Ltn1 in regulating mitogen-activated kinase signaling via regulatory RSK1/2 ubiquitylation. Taken together, our results suggest that mammalian RQC interactions are difficult to observe and may be more transient than the homologous complex in *S. cerevisiae* and that Ltn1 has RQC-independent functions.**

Monitoring Editor
Sandra Wolin
National Cancer Institute, NIH

Received: Dec 12, 2017
Revised: Mar 6, 2018
Accepted: Mar 9, 2018

INTRODUCTION

The successful decoding of mRNA into protein is not an error-free process. Errors during transcription, posttranscriptional mRNA processing, or translation can result in the production of defective nascent chains that require ubiquitin-mediated degradation (Drummond and Wilke, 2009; Lykke-Andersen and Bennett, 2014; Harper and Bennett, 2016). Ribosome-associated quality control mechanisms facilitate the triage and subsequent proteasome-dependent degradation of these potentially toxic defective translation products (Matsuda *et al.*, 2014; Brandman and Hegde, 2016; Joazeiro, 2017). One such mechanism involves the cotranslational recruitment of a ribosome quality control (RQC) complex to terminally stalled ribosomes (Brandman and Hegde, 2016; Joazeiro, 2017). Elegant biochemical and genetic characterization of the RQC has resulted in the following model. First, terminally stalled ribosomes are sensed by unknown mechanisms that result in the initial regulatory ubiquitylation of 40S ribosomal proteins in a ZNF598-dependent (Hel2 in *Saccharomyces cerevisiae*) manner (Garzia *et al.*, 2017; Juszkiewicz and Hegde, 2017; Matsuo *et al.*, 2017; Sundaramoorthy *et al.*, 2017). The alternative ribosome rescue factors, Hbs1L and Pelota (Hbs1 and Dom34 in *S. cerevisiae*), in concert with ABCE1 facilitate splitting of the 40S and 60S subunits allowing for mRNA destruction (Shoemaker *et al.*, 2010; Shoemaker and Green, 2012; Pisareva *et al.*, 2011; Tsuboi *et al.*, 2012). Previous studies have further identified RQC interacting proteins that can facilitate ribosome rescue and ribosome-quality control events (Ishimura *et al.*, 2014; Matsuo *et al.*, 2017). The ubiquitin ligase Ltn1, also known as Listerin, along with its cofactor nuclear export mediator factor (NEMF) (Rqc2/Tae2 in *S. cerevisiae*) ubiquitylates nascent

This article was published online ahead of print in MBoC in Press (http://www.molbiolcell.org/cgi/doi/10.1091/mbc.E17-12-0714) on March 22, 2018.

*Address correspondence to: Eric J. Bennett (e1bennett@ucsd.edu).

Abbreviations used: RQC, ribosome quality control complex; RSK, ribosomal protein S6 kinase.

chains trapped with the released 60S ribosomal subunit, which allows for subsequent p97/valosin-containing protein (VCP)-dependent (Cdc48 in *S. cerevisiae*) extraction and subsequent proteasomal degradation (Bengtson and Joazeiro, 2010; Brandman *et al.*, 2012; Defenouillere *et al.*, 2013; Shao *et al.*, 2013; Shao and Hegde, 2014; Verma *et al.*, 2013; Doamekpor *et al.*, 2016; Shcherbik *et al.*, 2016; Kostova *et al.*, 2017). Ltn1 has also been demonstrated to play a similar ribosome-associated quality control role with ribosomes docked at the ER or mitochondrial membranes during mitochondria and ER-localized protein transport (Crowder *et al.*, 2015; von der Malsburg *et al.*, 2015; Arakawa *et al.*, 2016; Izawa *et al.*, 2017). Interestingly, degron mapping in *S. cerevisiae* suggests that Ltn1 can target degron-containing proteins for destruction in a manner that is distinct from its well-characterized role in mediating RQC (Maurer *et al.*, 2016). Despite the rapidly expanding molecular knowledge of Ltn1 function in *S. cerevisiae*, a systematic characterization of the mammalian RQC or Ltn1 has yet to be described.

Mice lacking *listerin* with an intact RING domain die during embryonic development (Chu *et al.*, 2009). However, forward genetic approaches in mice revealed a hypomorphic mutation in the *listerin* gene that resulted in a neurodegenerative phenotype in which the mice display motor defects later in life due to motor neuron death (Chu *et al.*, 2009). Based on the well-characterized role for Ltn1 during ribosome-associated quality control, it is hypothesized that defective Ltn1 function in animals results in neurodegeneration through the accumulation of toxic defective translation products. In support of this hypothesis, mutations in mice that weaken translation fidelity or quality control mechanisms also result in neurodegeneration (Lee *et al.*, 2006; Ishimura *et al.*, 2014). Combined, these results suggest that elevating the levels of defective translation products beyond the capacity of quality control systems in neurons contributes to aging-associated degeneration. However, due to the lack of characterized endogenous Ltn1 substrates, it remains possible that other, uncharacterized RQC-independent Ltn1 functions contribute to the observed neurodegenerative phenotypes.

Here we utilize proximity-labeling proteomic approaches along with standard affinity-purification approaches to systematically characterize the core mammalian RQC complex. Surprisingly, interactions among the core RQC proteins Ltn1, p97/VCP, NEMF, and TCF25 were difficult to capture, even with proximity-labeling approaches. However, proximity-labeling identifies uncharacterized Ltn1 interacting proteins and we demonstrate that subsets of these are Ltn1 substrates. We show that Ltn1 can ubiquitylate members of the mammalian ribosomal S6 kinase family, RPS6KA1 and RPS6KA3 (also known as RSK1 and RSK2) in a regulatory and nondegradative manner. Loss of Ltn1 function results in elevated RSK1 activity, indicating that Ltn1 functions to restrict RSK1 activity. Taken together, we identify putative mammalian Ltn1 substrates and demonstrate that Ltn1 regulates mitogen-activated protein kinase (MAPK) signaling.

RESULTS

Utilization of proximity-labeling and traditional affinity-capture approaches to interrogate p97/VCP interacting proteins

Proximity-labeling approaches have been successfully utilized to characterize both interacting proteins for individual baits of interest and organelle proteomes (Kim and Roux, 2016). The BioID approach fuses a mutant version of the *Escherichia coli* biotin ligase, which prematurely releases activated biotinoyl-adenosine monophosphate (AMP), resulting in the biotinylation of neighboring interacting proteins (Roux *et al.*, 2012). The APEX approach adds an ascorbate peroxidase to proteins of interest that, on addition of biotin-phenol and hydrogen peroxide, allow for the rapid and temporal biotinylation of neighboring proteins via a biotin-phenoxyl radical intermediate and has been successfully utilized to characterize a variety of interactomes (Rhee *et al.*, 2013; Chen *et al.*, 2015; Lam *et al.*, 2015; Hung *et al.*, 2016, 2017; Loh *et al.*, 2016; Reinke *et al.*, 2017a,b; Bersuker *et al.*, 2018; Markmiller *et al.*, 2018). While the BioID approach has been used to identify substrates for the well-characterized βTRCP1/2 cullin-RING ubiquitin ligase complex (Coyaud *et al.*, 2015), the APEX-approach has not been previously used to capture ligase substrates. To systematically characterize the mammalian RQC complex, we first utilized both the BioID and APEX proximity-labeling approaches as well as standard affinity capture techniques to evaluate interacting partners for the well-characterized RQC factor p97/VCP. We first generated HEK293 cells with dox-inducible expression of FLAG-hemagglutinin (HA), FLAG-APEX2, or BirA-R118G (denoted as BirA* hereafter)-FLAG–tagged p97/VCP using the Flp-In system to achieve stable single site integration of our transgenes. Cell lines expressing similarly tagged green fluorescent protein (GFP) were generated to serve as specificity controls. Tagged protein expression was induced for 16 h, and for BirA*-FLAG–tagged GFP or p97/VCP-expressing cell lines, 50 μM biotin was added to the media. Protein biotinylation was induced in cell lines expressing FLAG-APEX2–tagged GFP or p97/VCP by adding biotin-phenol to the cells for 1 h prior to a 1-min addition of hydrogen peroxide. Subsequent analysis of whole-cell lysates by SDS–PAGE verified protein biotinylation in BirA* and APEX2-tagged samples but not in FLAG-HA–tagged samples (Figure 1A).

We employed a SILAC (stable isotope labeling with amino acids in cell culture) approach to identify specific p97/VCP interacting proteins. To accomplish this, we metabolically labeled control GFP-expressing cell lines with heavy $^{13}C^{15}N$-arginine and lysine. After induction of protein expression and proximity-labeling, an equal number of light-labeled p97/VCP-expressing cells were mixed with heavy-labeled GFP-expressing cells. Cells were lysed, and for BirA* and APEX2-tagged samples, biotinylated proteins were isolated by streptavidin agarose under native lysis and IP conditions. For FLAG-HA–tagged samples, interacting proteins were isolated by native anti-FLAG immunoprecipitation. Analysis of isolated proteins by mass spectrometry allowed for the identification of specific p97/VCP interacting proteins by examining the heavy:light (H:L) ratio of all identified and quantified proteins (Figure 1B and Supplemental Table S1). Proteins with a Log2 transformed (H:L) ratio below –1 in replicate samples were denoted as putative p97/VCP interacting proteins. All three approaches identified known p97/VCP interacting proteins (Figure 1, B and C, and Supplemental Figure S1A). However, the BioID approach routinely resulted in the identification of more known p97/VCP interactors including those recently shown to interact with p97/VCP with relatively weaker affinities (Figure 1C and Supplemental Figure S1, A and B) (Xue *et al.*, 2016). Each approach resulted in the identification of unique p97/VCP interacting proteins with surprisingly little overlap among the three approaches (Figure 1D). These results suggest, in agreement with previous studies (Coyaud *et al.*, 2015), that combining approaches results in the identification of both more known and putative interacting proteins for a given bait compared with any individual technique.

BioID identifies both known and uncharacterized Ltn1 interacting proteins

Ltn1 has a well-established role in ribosome-associated quality control, and the *S. cerevisiae* RQC complex has been previously biochemically characterized (Brandman *et al.*, 2012). To both verify the

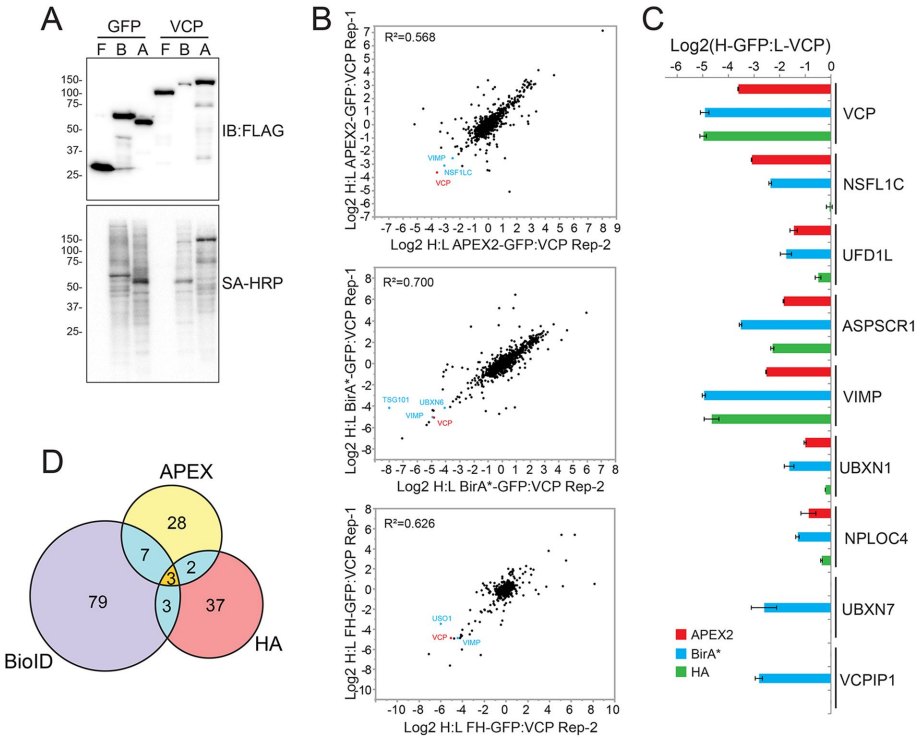

FIGURE 1: Utilization of three proteomic methods toward the identification of p97/VCP interacting proteins. (A) 293 Flp-In cells with dox-induced expression of FLAG-HA(F), BirA*-FLAG(B), or FLAG-APEX2(A)–tagged GFP or VCP were treated with doxycycline overnight. For BirA*-FLAG-GFP or VCP-expressing cells, 50 μM biotin was addd to the growth media for 16–20 h prior to cell harvesting. For FLAG-APEX2-GFP of VCP-expressing cells protein biotinylation was induced by addition of 500 μM biotin-phenol for 1 h followed by a 1-min treatment of 1.5 mM hydrogen peroxide. Whole-cell extracts were immunoblotted with α-FLAG antibodies or probed with streptavidin-conjugated horseradish peroxidase (SA-HRP). (B) Heavy-labeled GFP-expressing control cells were mixed with light-labeled VCP-expressing cells that were similarly tagged as indicated. Depicted is the scatter plot of log2 heavy to light (H:L) ratios of streptavidin or anti-FLAG–isolated and identified proteins from replicate experiments for APEX2 (top), BirA* (middle), or FLAG-HA–tagged VCP (bottom). The bait VCP protein is indicated in red, and known VCP interacting proteins are depicted in blue. For panels B–D, FLAG-HA and BirA* enrichments were performed in triplicate, and APEX-based experiments were performed in duplicate. (C) Log2 heavy to light (H:L) ratios for known VCP interacting proteins identified from FLAG-APEX2 (red)-, BirA*-FLAG (blue)-, or FLAG-HA (green)-expressing cell extracts is shown. Error bars represent SD of the ratios from triplicate (FLAG-HA, and BirA*-FLAG experiments) or duplicate (FLAG-APEX2) experiments. (D) Venn diagram depicting the overlap of identified VCP interacting proteins for each of the three proteomic platforms.

presence of an orthologous mammalian RQC complex and to identify new Ltn1 interacting proteins, we generated stable cell lines with inducible expression of FLAG-HA-, BirA*-FLAG-, or FLAG-APEX2–tagged Ltn1 in a manner identical to our p97/VCP-expressing cell lines. On the basis of the results obtained using p97/VCP, we utilized all three interaction mapping approaches to identify the greatest number of potential Ltn1 interacting proteins. We again used GFP-expressing cell lines as a specificity control but switched to a label-free proteomic approach to facilitate a simpler cell culture scheme. Ltn1 protein expression was significantly lower than GFP in all three cell lines, which resulted in reduced protein biotinylation for BirA*-FLAG- and FLAG-APEX2–tagged Ltn1-expressing lines compared with control GFP-expressing cell lines (Figure 2A). FLAG immunoprecipitations from cell lysates with FLAG-HA–tagged Ltn1 or GFP or streptavidin pull downs from lysates with BirA*-FLAG- or FLAG-APEX2–tagged Ltn1 or GFP were done in triplicate. Isolated proteins were identified by mass spectrometry, and high-confidence interacting proteins were annotated using a modified version of the CompPASS scoring matrix (Supplemental Table S2) (Sowa *et al.*, 2009). The known Ltn1 interacting protein NEMF was only identified from cells expressing BirA*-FLAG–tagged Ltn1 compared with p97/VCP, which was identified in all conditions in both GFP- and Ltn1-expressing cells (Figure 2B). Standard affinity-purification approaches identified the greatest number of putative Ltn1 interacting proteins (Figure 2C). Scoring of all putative Ltn1 interacting proteins identified using the BioID approach revealed NEMF to be the top-scoring protein (Figure 2D and Supplemental Table S2). Other top-scoring Ltn1 interacting proteins included four proteins implicated in tubulin glutamylation (LRRC49, NICN1, TPGS1, and TPGS2), two tRNA modification enzymes (TRMT2A and TYW3), and a p90 ribosomal S6 kinase (RPS6KA1) (Figure 2D). Interestingly, other putative mammalian RQC proteins, TCF25 and p97/VCP, as well as 60S ribosomal proteins were not identified as specific Ltn1 interacting proteins.

Previous studies have demonstrated that the RQC complex composed of Ltn1, Rqc2/Tae2, Rqc1, and Cdc48 can be isolated from *S. cerevisiae* extracts using epitope-tagged Rqc1 (Brandman *et al.*, 2012). Further, studies in mammalian cells demonstrated that Ltn1 shifted from a ribosome-free fraction to a 60S containing sucrose-density fraction on cycloheximide treatment to cells prior to fractionation (Shao *et al.*, 2013). Taken together, it is possible that we were unable to detect the mammalian RQC due to our use of tagged Ltn1 isolated from untreated cells. To systematically examine the network of RQC interactions in mammalian cells, we generated cell lines with dox-inducible expression of FLAG-HA–tagged TCF25 (putative Rqc1 homologue) and NEMF (Rqc2/Tae2 in *S. cerevisiae*). We also generated cell lines expressing Ltn1 lacking its C-terminal RING domain (ΔRING) to examine whether expression of a catalytically inactive version of Ltn1 resulted in capture of known RQC components or putative substrates. These new cell lines were generated using the same Flp-In approach utilized for the other tested RQC components. We used sucrose-density gradient fractionation to determine if putative RQC components were present in ribosome containing fractions in extracts from untreated and cycloheximide (CHX)-treated cells. Both exogenous and endogenous Ltn1, as well as exogenous TCF25 and NEMF, were primarily present in fractions that were devoid of 60S and 80S ribosomes in untreated FLAG-HA-Ltn1–, FLAG-HA-TCF25–, or FLAG-HA-NEMF–expressing cells (Figure 3A). Cycloheximide treatment resulted in variable shifting of endogenous Ltn1 into ribosome-containing fractions, whereas the distribution of exogenous Ltn1, TC25, and NEMF was largely unchanged on CHX treatment with most of the protein present in ribosome-free fractions (Figure 3A). Previous studies

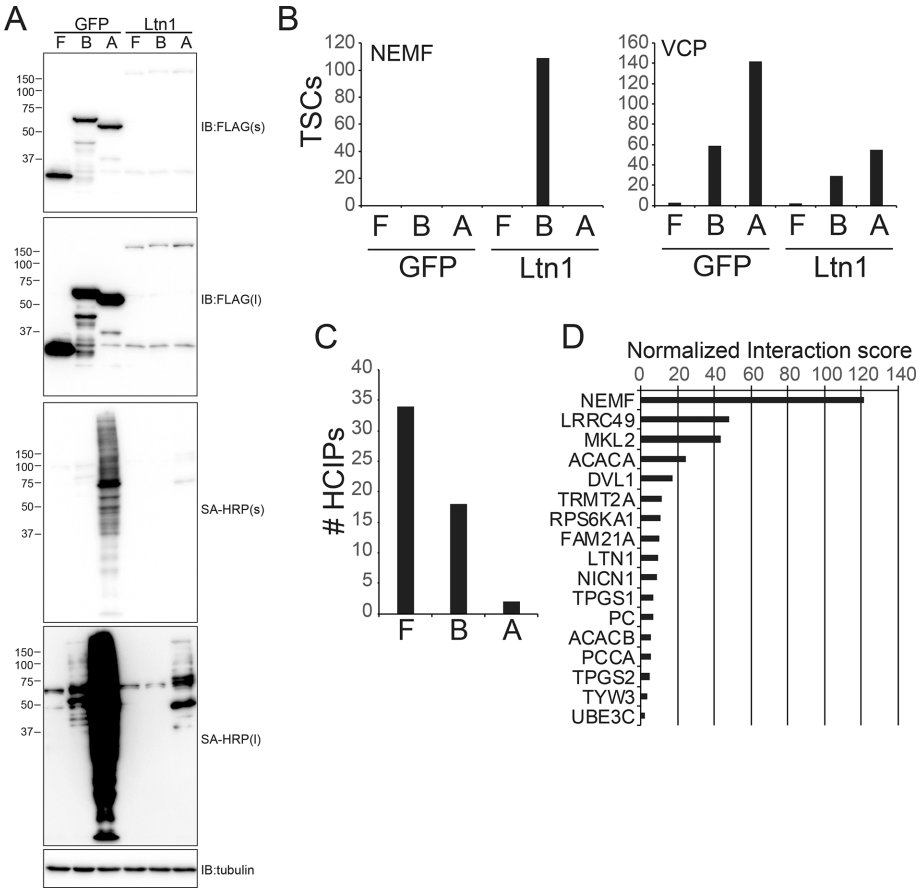

FIGURE 2: Identification of Ltn1-interacting proteins using proximity labeling approaches. (A) 293 Flp-In cells with dox-induced expression of FLAG-HA(F)-, BirA*-FLAG(B)-, or FLAG-APEX2(A)–tagged GFP or Ltn1 were treated with doxycycline overnight, and protein biotinylation was induced as described for BirA*- or APEX2-tagged cell lines. Whole-cell extracts were immunoblotted with a-FLAG antibodies or probed with SA-HRP. Short (s) or long (l) exposures are depicted. (B) The summed total spectral counts (TSCs) from replicate experiments corresponding to NEMF (left) or VCP (right) from streptavidin or anti-FLAG–isolated and identified proteins from FLAG-HA(F)-, BirA*-FLAG(B)-, or FLAG-APEX2(A)–tagged GFP- or Ltn1-expressing cell extracts. For panels B–D, all IPs were performed in triplicate from distinct experiments and cell lysates. (C) The number of high-confidence interacting proteins (HCIPs) for Ltn1 for each of the three proteomic platforms was determined using a modified CompPASS scoring method. (D) The normalized interaction scores as determined by the CompPASS scoring method for top-scoring Ltn1 interacting proteins identified using the BioID approach is shown.

have demonstrated that the 40S protein Rps3 becomes monoubiquitylated on CHX-induced translation elongation inhibition (Higgins *et al.*, 2015). We observe this Rps3 ubiquitylation event that confirms successful translation elongation inhibition in CHX-treated cells. We then determined the interaction landscape of each RQC protein with and without CHX treatment using FLAG immunoprecipitations from native whole-cell extracts (Figure 3, B and C, and Supplemental Table S3). Compared to control cells expressing GFP, we detected a CHX-inducible interaction between Ltn1 and NEMF using either Ltn1 or NEMF as the bait protein (Figure 3D). An interaction between TCF25 and NEMF was also observed but in a CHX-independent manner, and no specific interaction with p97/VCP, 40S ribosomal proteins, 60S ribosomal proteins, or other translation initiation factors was observed with any RQC protein (Figure 3, D and E, and Supplemental Table S3). Together, these results indicate that the interaction with Ltn1 and NEMF can be stimulated by translation elongation inhibition. Further, the majority of Ltn1 in 293T cells is not found in ribosome-containing fractions, which suggests mammalian Ltn1 may have ribosome-independent functions. While it is possible that the mammalian RQC complex is less biochemically stable compared with its counterpart in *S. cerevisiae*, we cannot rule out the possibility that overexpression of one or multiple RQC factors may result in altered complex stoichiometry and possible RQC destabilization.

Ltn1 ubiquitylates TYW3 and RSK1/2 in a regulatory manner

We first sought to validate the Ltn1 interacting proteins identified by the BioID approach. To accomplish this, we generated cell lines expressing dox-inducible BirA*-FLAG–tagged LRRC49, NICN1, TTLL1, RSK2 (RPS6KA3), or TYW3 (Figure 4A) using 293 Flp-In cells. We also generated a cell line expressing BirA*-FLAG–tagged Ltn1 that lacks its RING domain to determine whether any of the observed Ltn1 interactions were ubiquitin ligase activity dependent. Replicate BioID analysis of wild type and ΔRING Ltn1 confirmed the originally identified Ltn1 interactions and demonstrated these interactions to be independent of the RING domain within Ltn1 (Figure 4B). BioID analysis of putative Ltn1 interacting proteins demonstrated that RSK2 and TYW3 interacted with Ltn1 in a reciprocal manner (Figure 4C and Supplemental Table S4). Despite validating the interaction between members of the tubulin glutamylation complex (Figure 4D), we were unable to detect an interaction between Ltn1 and any of the glutamylation factors (LRRC49, NICN1, or TTLL1) at a level greater than that observed in BirA*-GFP-expressing cells (Figure 4, B and D). These results suggest that the association between Ltn1 and glutamylation factors may be driven by the overexpression of Ltn1 or may be otherwise enhanced by the localization and abundance of BirA*-FLAG–tagged Ltn1. Despite the inability to validate the interaction with Ltn1 and the tubulin glutamylation factors, we were able to validate the interaction between Ltn1 and p90 ribosomal S6 kinases as well as with TYW3.

To determine whether Ltn1 can ubiquitylate the identified interacting proteins, we transiently transfected myc-tagged versions of putative Ltn1 substrates along with HA-tagged ubiquitin in HEK293 cells with stable and dox-inducible expression of either wild type or ΔRING Ltn1. Ubiquitylating proteins were isolated under native conditions by HA immunoprecipitation, and the presence of putative Ltn1 substrates was probed using myc immunoblots. High-molecular-weight forms, which are presumably ubiquitylated RSK1, RSK2, and TYW3, could be observed within whole-cell extracts as well as HA immunoprecipitates (Figure 5A). The ubiquitylation of myc-tagged RSK1, RSK2, and TYW3 observed in whole-cell extracts were dependent on expression of wild-type Ltn1 as expression of ΔRING Ltn1 did not support ubiquitylation of exogenously expressed RSK1, RSK2, or TYW3 (Figure 5A). In comparison, ubiquitylation of myc-tagged

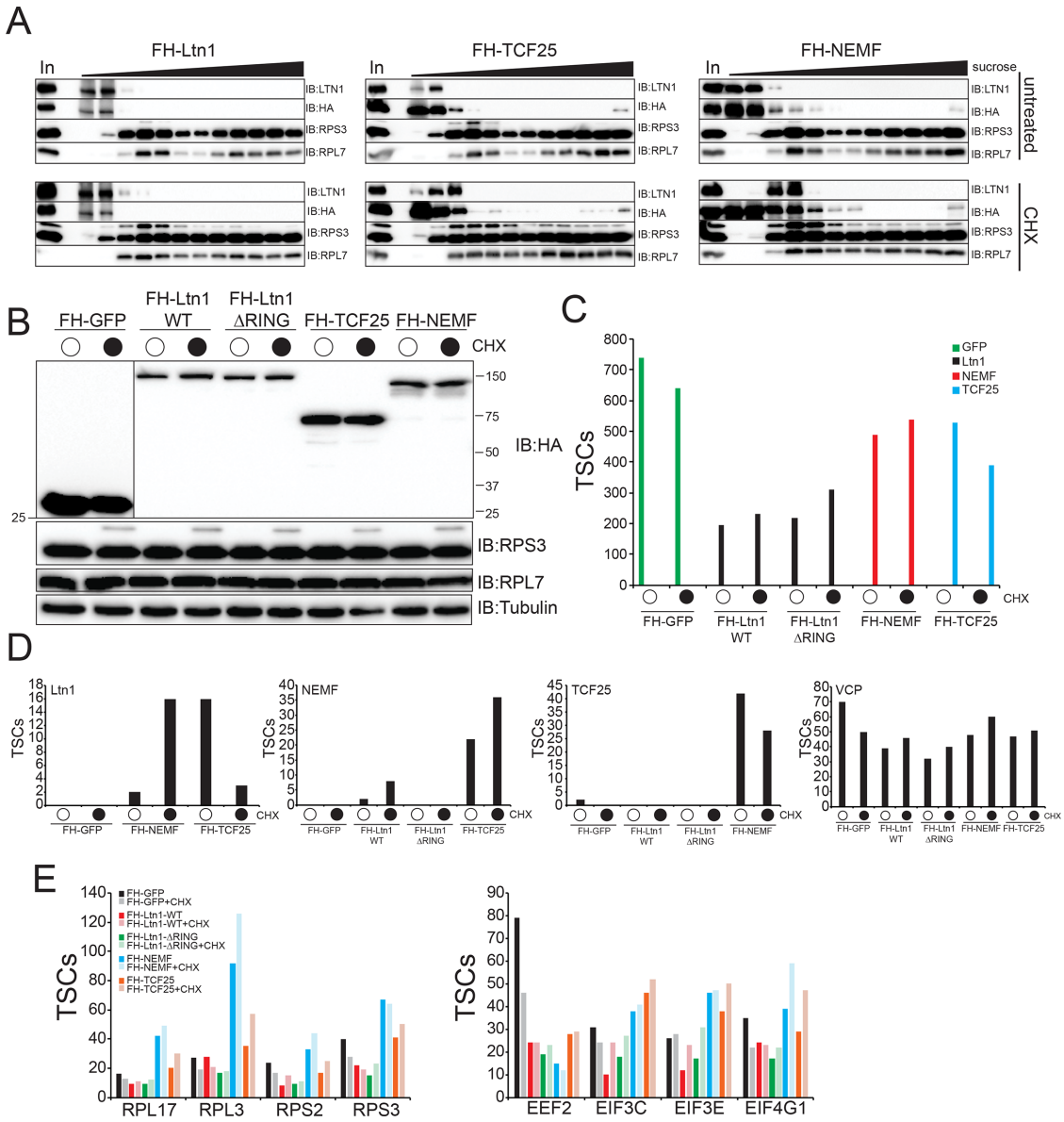

FIGURE 3: Systematic proteomic interrogation of the mammalian RQC complex. (A) 293 Flp-In cells with dox-induced expression of FLAG-HA (FH)–tagged Ltn1 or TCF25, or 293T cells with constitutive stable-expression of FLAG-HA–tagged NEMF, were either untreated (top) or treated with 100 µg/ml cycloheximide (CHX, bottom) for 1 h. Native cell extracts were separated on a 5–45% linear sucrose gradient. Inputs (In) and isolated fractions across the gradient were immunoblotted as indicated. Note the appearance of the slower migrating ubiquitylated RPS3 in CHX-treated samples as a marker for CHX treatment. (B) 293 Flp-In cells with dox-induced expression of the indicated FH-tagged proteins were either untreated (top) or treated with 100 µg/ml cycloheximide (CHX, bottom) for 1 h. Whole-cell extracts were immunoblotted as indicated. (C) Total spectral counts (TSCs) to the corresponding bait proteins from anti-HA–isolated proteins from cell lines expressing the indicated FH-tagged proteins is depicted. (D) Total spectral counts (TSCs) corresponding to identified Ltn1, NEMF, TCF25, or VCP from anti-HA–isolated proteins from the indicated FH-tagged protein expressing cell extracts. Cells were either untreated or treated with CHX as indicated. (E) Total spectral counts (TSCs) corresponding to the indicated representative proteins for 40S, 60S, and translation initiation factors identified from either untreated or CHX-treated cells from FH-tagged GFP (black)-, wild type Ltn1 (red)-, ΔRING Ltn1 (green)-, NEMF (blue)-, or TCF25 (orange)-expressing cells. For panels C–E, summed TSCs are shown from triplicate runs of individual experiments.

TTLL1 was only minorly altered by ΔRING Ltn1 expression, and NICN1 ubiquitylation was completely unchanged by ΔRING Ltn1 expression. The presence of the monomeric and unmodified myc-tagged proteins in HA immunoprecipitates suggests that a portion of these proteins may interact with ubiquitin in noncovalent manner and possibly as part of a larger complex. However, the presence of high-molecular-weight modified forms of RSK1, RSK2, and TYW3 in whole-cell extracts and HA immunoprecipitates that are observed only on expression of wild type and not inactive Ltn1 suggests that Ltn1 can ubiquitylate these proteins within cells.

Ltn1 ubiquitylation of RSK1, RSK2, and TWY3 could either result in degradation or impart a regulatory function on target proteins

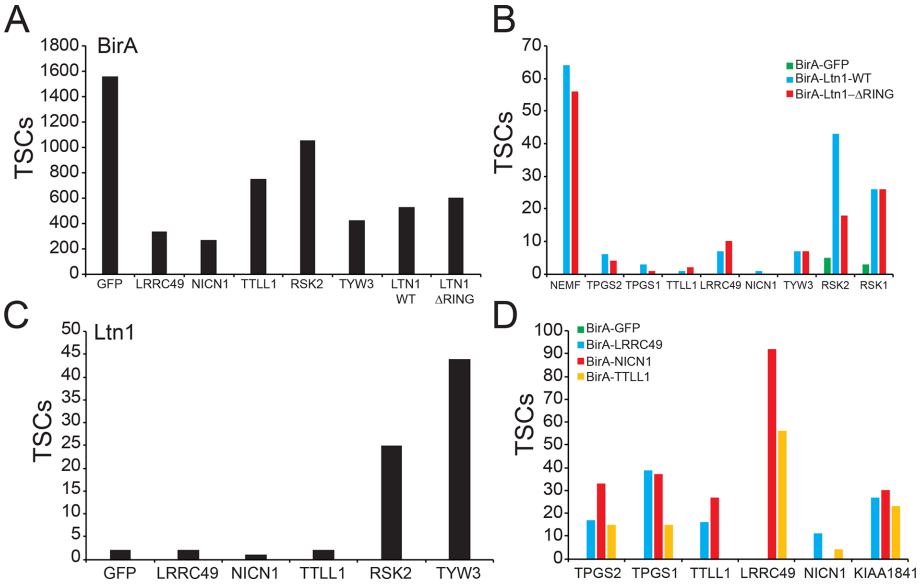

FIGURE 4: Validation of candidate Ltn1 interacting proteins. (A) 293 Flp-In cells with dox-induced expression of the indicated BirA*-FLAG–tagged proteins were generated. Total spectral counts (TSCs) corresponding to BirA (bait) from streptavidin-isolated proteins from each of the eight dox-inducible cell lines. (B) Total spectral counts (TSCs) corresponding to the indicated proteins isolated from streptavidin pull downs from BirA*-tagged GFP (green)-, wild-type Ltn1 (blue)-, or ΔRING Ltn1 (red)-expressing cells. The identified protein in indicated on the x-axis. (C) Total spectral counts (TSCs) corresponding to Ltn1 from streptavidin-isolated proteins from the indicated BirA*-FLAG–tagged protein-expressing cell lines. The different pull downs for separate cell lines are indicated on the x-axis. (D) Total spectral counts (TSCs) corresponding to the indicated proteins isolated from streptavidin pull-downs from BirA*-tagged GFP (green)-, LRRC49 (blue)-, NICN1 (red)-, or TTLL1 (orange)-expressing cells. TSCs corresponding to the bait proteins were omitted to allow for easier visualization of interactions between complex members. The identified protein in indicated on the *x*-axis. For all panels, summed TSCs are shown from triplicate runs of individual experiments.

distinct from degradation. To differentiate between these two possibilities, we determined if the steady-state abundance of putative Ltn1 substrates was altered on loss of Ltn1 function as would be expected for degradation-based ubiquitylation. The steady-state protein levels of either exogenous or endogenous RSK1, RSK2, and TTLL1 were unchanged on small interfering RNA (siRNA)-mediated knockdown of Ltn1 (Figure 5, B and C). Further, exogenous TYW3 steady-state protein levels were similarly unaltered on Ltn1 knockdown (Figure 5B). We then directly examined protein turnover dynamics using cycloheximide time-course experiments to confirm that loss of Ltn1 did not result in delayed protein turnover of putative substrates. Knockdown of Ltn1 using multiple siRNAs in our HEK293 cell lines with dox-inducible expression of RSK2, TTLL1, or TYW3 did not result in delayed degradation kinetics of any of the tested substrates (Figure 5D). There appeared to be a slight acceleration of FLAG-HA–tagged TTLL1 protein degradation on Ltn1 knockdown (Figure 5D). We also did not observe any alteration in the protein degradation kinetics of endogenous RSK1 in either 293T or HCT116 cells on Ltn1 knockdown (Figure 5E). Taken together, our results indicate that Ltn1 can ubiquitylate RSK1, RSK2, and TYW3, and this ubiquitylation does not function to target these proteins for degradation.

Ltn1 regulates RSK1/2 activity on mitogen-activated cell signaling

Because knockdown of Ltn1 did not alter RSK1 or RSK2 protein turnover, we examined if RSK1/2 activity was altered on loss of Ltn1 function. First, we established an RSK1/2 activity assay. A bevy of substrates for RSK1/2 have been previously described (Sapkota *et al.*, 2007; Romeo *et al.*, 2012). Many RSK1/2 substrates are not exclusive to RSK1/2 and can be phosphorylated by other kinases, which can complicate an analysis of RSK1/2 activity using these substrates. For instance, RSK1/2 can phosphorylate RPS6 on serine 235 and 236 but these same sites are also phosphorylated by p70 S6 kinase. In searching for exclusive RSK1/2 targets, a previous study demonstrated that RSK1/2 can phosphorylate TSC2 at serine 1798 and that this site was distinct from other mTOR-dependent TSC2 phosphorylation events (Roux *et al.*, 2004). To independently evaluate this TSC2 phosphorylation event, we treated 293T cells with increasing concentrations of the mTOR inhibitors rapamycin and Torin-1, as well as a potent AKT1 inhibitor (MK2206). The levels of phosphorylated RPS6 (S6) and p70 S6 kinase (S6K) were reduced on rapamycin, Torin-1, and MK2206 (AKT inhibitor), demonstrating the efficacy of these inhibitors as well as establishing that RPS6 phosphorylation could not be used to directly examine RSK1/2 activity. Further, Torin-1 and AKT inhibition resulted in a reduction of ERK1/2 phosphorylation, indicating that these inhibitors widely impact mitogen-activated protein kinase (MAPK) signaling in otherwise unperturbed cells. However, rapamycin, Torin-1, or MK2206 treatment did not reduce S1798 TSC2 phosphorylation in unperturbed cells, indicating that this phosphorylation event was not impacted by mTOR or AKT1 signaling (Figure 6A). We then tested the impact of these same mTOR and AKT1 inhibitors on overt activation of MAPK signaling in serum-starved cells by the addition of phorbol ester (phorbol 12-myristate 13-acetate [PMA]). PMA treatment in serum-starved cells resulted in robust phosphorylation of ERK1/2 as well as increased phosphorylation of TSC2 (S1798) in a manner that was unaltered by mTOR or AKT1 inhibition (Figure 6B). RSK1 phosphorylation itself was also stimulated by PMA treatment but this phosphorylation was unaffected by mTOR or AKT1 inhibition (Figure 6B). Phosphorylation of S6K and 4EBP was substantially reduced by Torin-1 treatment as expected, but RPS6 phosphorylation itself, while reduced on mTOR or AKT1 inhibition, was not completely abolished in serum-starved and PMA-activated cells (Figure 6B). Addition of the RSK1 inhibitor BI-D1870 to serum-starved and PMA-activated cells completely blocked TSC2 S1798 phosphorylation without impacting upstream ERK1/2 or RSK1 phosphorylation or the mTOR-dependent S6K phosphorylation (Figure 6C) (Sapkota *et al.*, 2007). Interestingly, RPS6 phosphorylation was reduced by either Torin-1 or BI-D1870, indicating that multiple kinases can generate this phosphorylation event (Figure 6C). Consistent with previous results, our data indicate that TSC2 phosphorylation at S1798 can be used as a specific RSK1/2 activity assay.

To determine whether Ltn1 regulates RSK1/2 activity, we knocked down Ltn1 expression and examined MAPK signaling in serum-starved cells activated with PMA. Loss of Ltn1 expression resulted in increased TSC2 phosphorylation compared with controls without

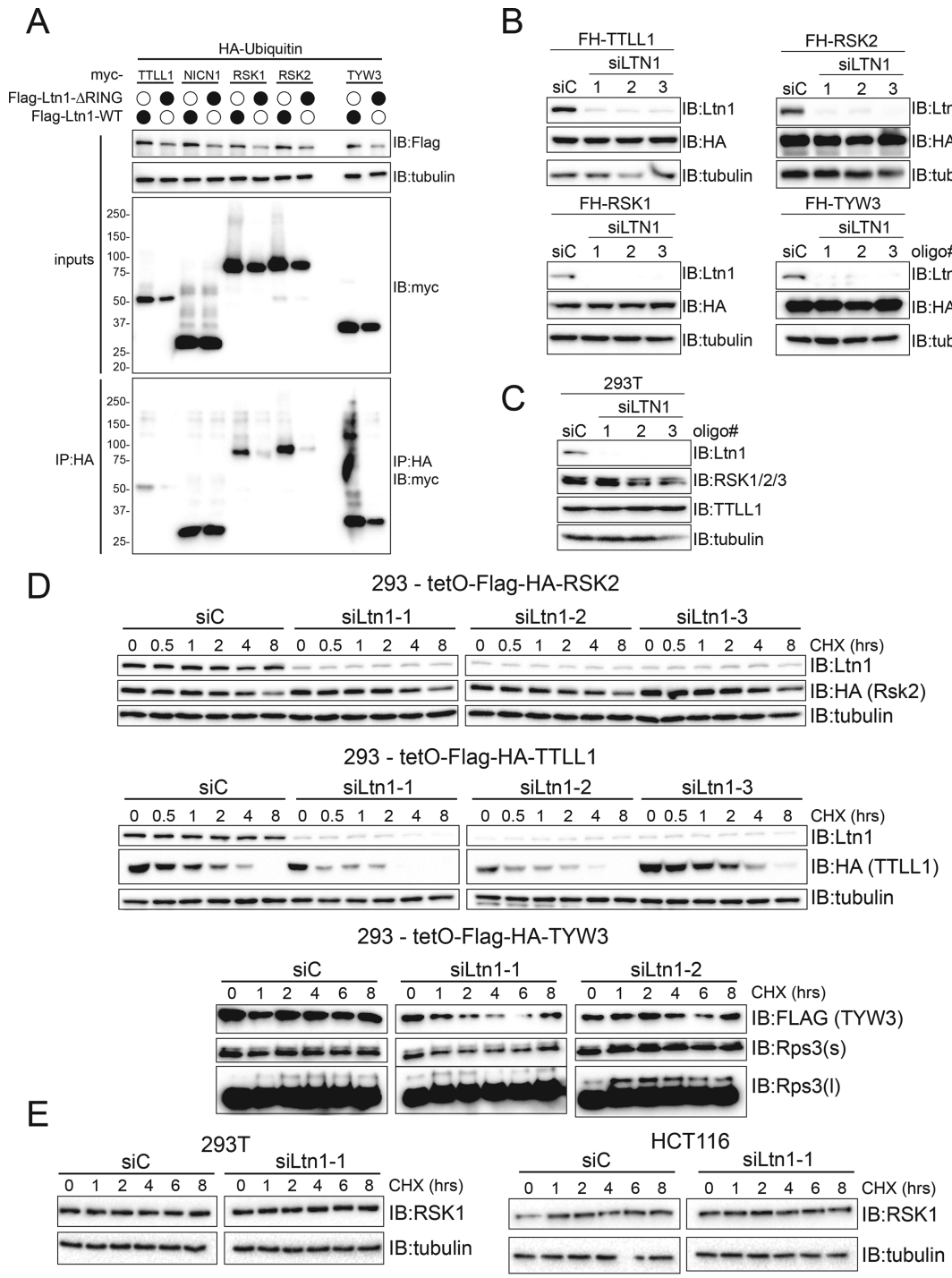

FIGURE 5: Ltn1 ubiquitylates a subset of identified interacting proteins in a regulatory manner. (A) 293 Flp-In cells with dox-induced expression of FLAG-HA–tagged wild type or ΔRING Ltn1 were transfected with HA-ubiquitin and the indicated myc-tagged Ltn1 interacting protein. Whole-cell lysates or anti-HA immune-complexes isolated under native conditions were immunoblotted as indicated. (B) 293 Flp-In cells with dox-induced expression of the indicated FLAG-HA (FH)-tagged proteins were transfected with control scrambled siRNA oligos (siC) or three separate Ltn1-targeting siRNA oligos. Whole-cell extracts were immunoblotted as indicated. (C) 293T cells were transfected with control scrambled siRNA oligos (siC) or three separate Ltn1-targeting siRNA oligos. Whole-cell extracts were immunoblotted as indicated. (D) 293 Flp-In cells with dox-induced expression of FLAG-HA–tagged RSK2, TTLL1, or TYW3 were transfected with control scrambled siRNA oligos (siC) or Ltn1-targeting siRNA oligos. Seventy-two hours after siRNA transfection, cells were either untreated or treated with 100 μg/ml cycloheximide (CHX) for the indicated times. After treatment, cells were harvested and whole-cell extracts were immunoblotted as indicated. (E) 293T cells (left) or HCT116 cells (right) were transfected with control scrambled siRNA oligos (siC) or Ltn1-targeting siRNA oligos. Seventy-two hours after siRNA transfection, cells were either untreated or treated with 100 μg/ml cycloheximide (CHX) for the indicated times. After treatment, cells were harvested, and whole-cell extracts were immunoblotted as indicated.

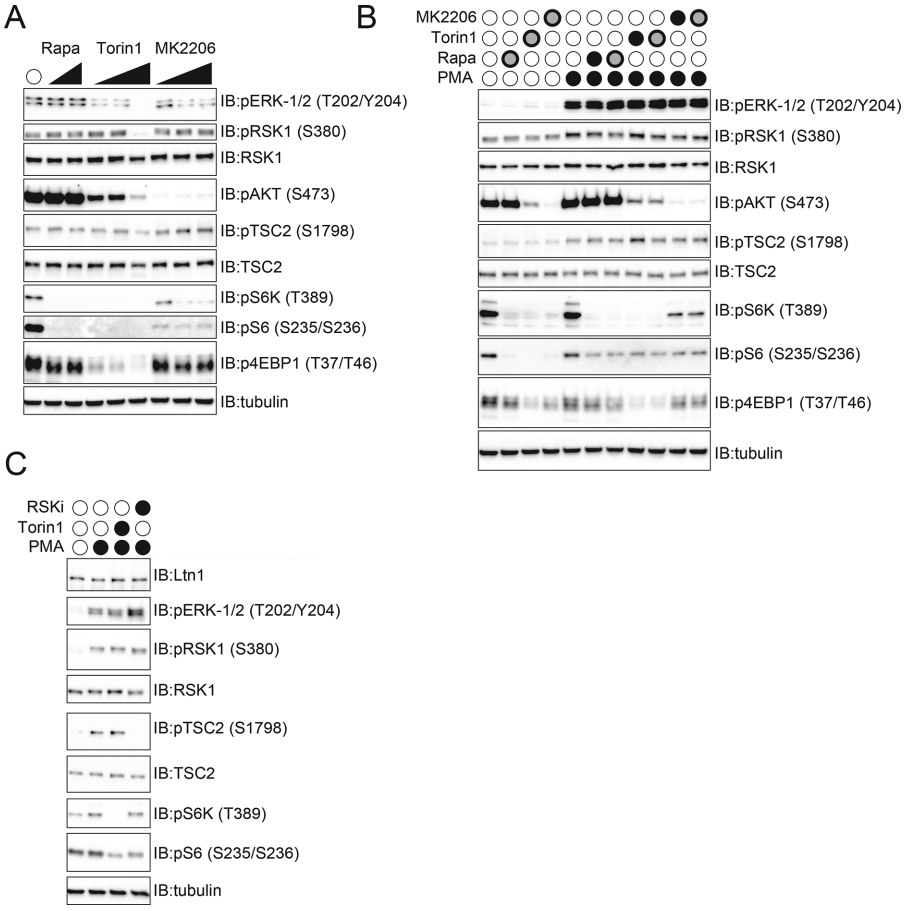

FIGURE 6: Validation of RSK1/2-dependent TSC2 phosphorylation at serine 1798. (A) 293T cells were treated with increasing concentrations of rapamycin, Torin 1, or the AKT1 inhibitor MK2206 for 1 h. Whole-cell extracts were immunoblotted as indicated. (B) 293T cells were serum starved overnight and were then treated with rapamycin, Torin 1, or MK2206 as indicated for 1 h prior to PMA addition for 15 min. After the 15-min PMA treatment, cells were harvested on ice, and whole-cell extracts were immunoblotted as indicated. Filled black circles indicate the following drug concentrations: PMA, 1 μM; rapamycin, 100 nM; torin-1, 100 nM; MK2206, 1 μM. Black outlined gray circles indicate the following drug concentrations: PMA, 1 μM; rapamycin, 250 nM; torin-1, 250 nM, MK2206, 5 μM. (C) 293T cells were serum starved overnight and were then treated with Torin-1 or RSK inhibitor (RSKi, BI-D1870) as indicated for 1 h prior to PMA addition for 15 min. Whole-cell extracts were immunoblotted as indicated. Filled black circles indicate the following drug concentrations: PMA, 1 μM; torin-1, 100 nM; RSKi, 10 μM.

altering upstream MAPK signaling (Figure 7A). Consistent with our previous results, loss of Ltn1 did not alter the abundance of RSK1. We validated that loss of Ltn1 resulted in elevated RSK1/2 activity in replicate experiments, as well as confirmed that the observed PMA-induced TSC2 phosphorylation was independent of mTOR activity but completely dependent on RSK1/2 activity (Figure 7, B and C). Summing together data from replicate experiments revealed a consistent elevation of phosphorylated TSC2 relative to total TSC2 levels on Ltn1 knockdown using three separate siRNA oligos (Figure 7C). To determine whether the observed Ltn1-dependent regulation of RSK1 signaling was associated with other RQC factors, we examined RSK1/2 activity on NEMF knockdown. The PMA-induced, RSK1/2-dependent TSC2 phosphorylation was largely unperturbed by loss of NEMF function, suggesting that Ltn1-mediated regulation of RSK1/2 activity was separable from its RQC function (Figure 7D). We confirmed the efficacy of the NEMF knock down by examining the levels of BirA*-FLAG-NEMF in 293 Flp-In cell lines after overnight dox treatment (Figure 5E). Taken together, our results both demonstrate that the BioID approach successfully identified uncharacterized Ltn1 substrates and suggest that Ltn1-dependent, regulatory ubiquitylation of RSK1/2 normally restrains RSK1 activity during MAPK signaling. Our results also demonstrate a possible ribosome-independent role for Ltn1 in regulating the activity of diverse substrates.

DISCUSSION

Proximity-labeling approaches can identify transient interacting proteins for ubiquitin-pathway components

Standard affinity-capture approaches or other substrate-trapping methods coupled with mass spectrometry have been widely used to identify candidate substrates for ubiquitin ligases of interest (Iconomou and Saunders, 2016; O'Connor and Huibregtse, 2017). Proximity labeling techniques allow for the irreversible biotinylation of neighboring proteins that potentially offer the advantage of capturing transient interacting proteins that do not stably associate with ubiquitin ligases and would be difficult to capture using standard affinity capture approaches (Hung *et al.*, 2016; Kim and Roux, 2016; Hesketh *et al.*, 2017). The utility of both BioID and APEX approaches have been robustly demonstrated to identify interactomes for diverse proteins in diverse organisms (Rhee *et al.*, 2013; Chen *et al.*, 2015; Lam *et al.*, 2015; Hung *et al.*, 2016, 2017; Loh *et al.*, 2016; Lobingier *et al.*, 2017; Reinke *et al.*, 2017a,b). Here we utilized both BioID and APEX techniques in addition to standard affinity-capture approaches toward the identification of interacting proteins for cytoplasmic localized ubiquitin pathway components. Each of the three proteomic platforms employed in this study identified known interacting partners for p97/VCP. However, BioID routinely resulted in the identification of more known interactors for p97/VCP and Ltn1. Interestingly, there was little overlap in the interactomes identified by each technique, suggesting that the parallel use of all three techniques can be used to identify larger numbers of putative ligase substrates. While BioID seemingly outperformed APEX and affinity-capture methods, a caveat of the BioID approach is that it is limited to steady-state conditions and is therefore unsuitable for the study of dynamic changes in interactomes in response to cell stimuli. The continued development of biotin ligase variants that can be used in the BioID approach will likely improve this method to allow greater temporal control over labeling conditions. Currently, because of the short labeling time scales, APEX-based methods are better suited to study protein interaction dynamics (Lobingier *et al.*, 2017). Compared to other proteomic methods, APEX-based approaches did not identify the most known or novel interactors for the cytoplasmic proteins tested here. However, this result could very well be restricted to the proteins tested here as we and others have successfully utilized APEX for to map a diversity of interactomes. A

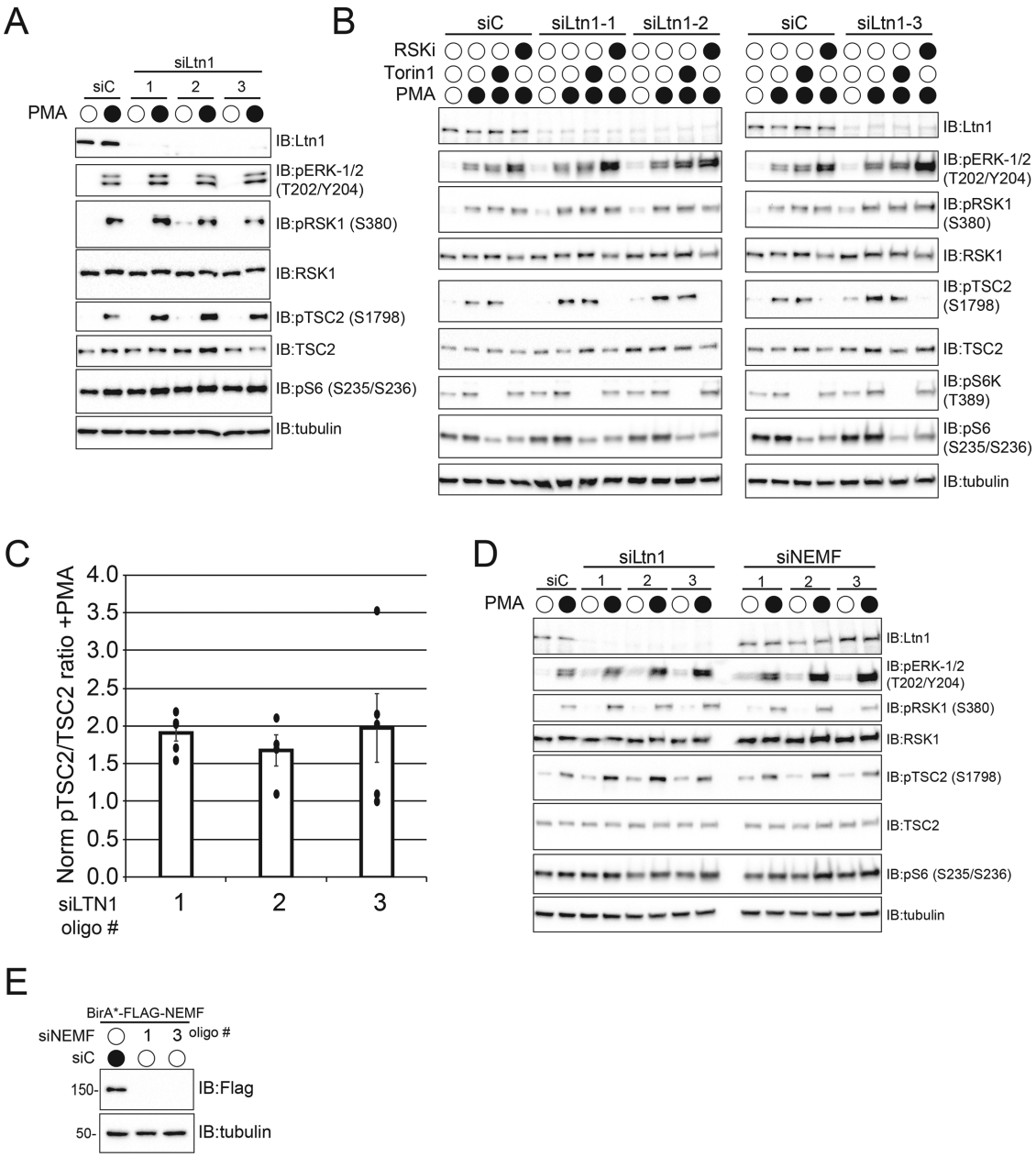

FIGURE 7: Ltn1 activity regulates RSK1/2 signaling. (A) 293T cells were transfected with control siRNA oligos (siC) or three separate Ltn1-targeting siRNA oligos. Two days after transfection, cells were serum starved overnight and were then untreated or treated with 1 μM PMA for 15 min. Whole-cell extracts were immunoblotted as indicated. (B) 293T cells were transfected with control siRNA oligos (siC) or three separate Ltn1-targeting siRNA oligos. Two days after transfection, cells were serum starved overnight and were then treated with 100 nM Torin 1 or 10 μM RSK inhibitor (RSKi) as indicated for 1 h prior to PMA treatment for 15 min. Whole-cell extracts were immunoblotted as indicated. (C) The band intensities from immunoblots from replicate experiments in 293T cells where Ltn1 was knocked down with individual siRNA oligos and the levels of pTSC2 (S1798) and total TSC2 were measured on serum starvation and subsequent PMA addition were quantified using Image Lab software volume tools (Bio-RAD). All immunoblots were imaged using a ChemiDoc XRS+ system which uses a charged-coupled device (CCD) detection system. A ratio of the background corrected band intensities of pTSC2:TSC2 was generated for each siRNA oligo targeting Ltn1 and normalized to the ratio observed in siControl-treated cells. Error bars represent SD ($N = 5$ for siLtn1 oligo 1 and 3, $N = 4$ for siLtn1 oligo 2). (D) 293T cells were transfected with control siRNA oligos (siC) or three separate oligos targeting Ltn1 or NEMF. Two days after transfection, cells were serum starved overnight and were then untreated or treated with 1 μM PMA for 15 min. Whole-cell extracts were immunoblotted as indicated. (E) 293 Flp-In cells with dox-induced expression of BirA*-FLAG-NEMF were transfected with control scrambled siRNA oligos (siC) or NEMF-targeting siRNA oligos. Forty-eight hours after siRNA transfection, BirA*-FLAG-NEMF expression was induced with dox for 16 h before cells were harvested. Whole-cell extracts were immunoblotted as indicated.

more complete and careful comparison of these methods with diversely localized bait proteins is needed to more fully evaluate the strengths and weaknesses of each approach.

Ribosome-independent roles for Ltn1

Ltn1 has a clear role in ribosome-associated quality control and has been repeatedly shown to mediate destruction of model defective nascent substrates within *S. cerevisiae* and human cells as well as in vitro (Brandman and Hegde 2016). Subsequent structural studies nicely define how the extended structure of Ltn1 results in binding to separated 60S ribosomal subunits allowing Ltn1, in concert with NEMF (Rqc2/Tae2), to both contact the exposed 40S interaction surface of the 60S particle and position the RING domain of Ltn1 near the ribosome nascent chain exit tunnel (Lyumkis *et al.*, 2014; Shao *et al.*, 2015; Shen *et al.*, 2015; Doamekpor *et al.*, 2016). Further, loss of Ltn1 function in *S. cerevisiae* results in Rqc2/Tae2-dependent carboxy-terminal extension of nascent chains by addition of alanine and threonine residues (CATylation) and subsequent protein aggregation (Choe *et al.*, 2016; Yonashiro *et al.*, 2016). These results suggest that RQC functions to both drive Ltn1-dependent nascent chain destruction and to engage with chaperone systems when Ltn1 fails. However, most of the in vivo studies characterizing Ltn1 and RQC function have been done in *S. cerevisiae*, and CATylation has only been demonstrated in *S. cerevisiae*. Further, quantitative proteomic studies in a range of human cell lines indicate that ribosomes are 100× more abundant than Ltn1, suggesting that Ltn1 capacity during RQC events is limited in mammalian cells (Wisniewski *et al.*, 2014; Harper and Bennett, 2016). Our results demonstrate that a substantial portion of mammalian Ltn1 is not ribosome associated at steady state or on complete inhibition of translation elongation. Further, proteomic characterization of mammalian Ltn1 interacting proteins using either affinity capture or proximity-labeling techniques did not identify ribosomal proteins as specific Ltn1 interactors. It is possible this interaction cannot be sampled due to limitations in the approaches utilized here. However, our data suggest that, along with its well-characterized RQC role, Ltn1 may have ribosome-independent functions.

Protein homeostasis modification through Ltn1-mediated regulatory ubiquitylation

Mammalian Ltn1 (Listerin) was first characterized through a murine forward genetic screen to identify genes involved in neurodegeneration (Chu *et al.*, 2009). This study identified hypomorphic mutations in *Listerin* that resulted in progressive neuronal death and motor-neuron dysfunction (Chu *et al.*, 2009). Subsequent elucidation of the role Ltn1 plays in ribosome-associated quality control led to the speculation that the accumulation of defective nascent chains in the absence of Ltn1 function contributed to the neurodegenerative phenotype observed in *lister* mice. However, the lack of characterized endogenous Ltn1 substrates has prevented a careful examination of whether Ltn1's RQC function or another undetermined Ltn1 function contributes to the observed neurological phenotype. Our results present a new role for Ltn1 outside of its known RQC function. Our results highlight an uncharacterized regulatory interaction between Ltn1 and the p90 ribosomal S6 kinases RSK1 and RSK2. These cytosolic kinases regulate many cellular functions, including cell cycle, proliferation, and mRNA translation (Romeo *et al.*, 2012; Lara *et al.*, 2013). Our data suggest that regulatory, nondegradative Ltn1-mediated ubiquitylation inhibits RSK1/2 activity. As such, loss of Ltn1 may result in unrestrained RSK1/2 activity during MAPK signaling and may drive translation during conditions that would otherwise restrain protein production. Ltn1-mediated regulatory ubiquitylation was also observed for TYW3, which operates within a conserved multienzyme cascade that catalyzes wybutosine modification of phenylalanine-decoding tRNAs (Noma *et al.*, 2006; Perche-Letuvee *et al.*, 2014). How Ltn1-mediated regulatory ubiquitylation impacts TYW3 function is unknown, but this observation provides another example of how non-ribosome-associated Ltn1 may regulate protein homeostasis in noncanonical ways.

MATERIALS AND METHODS

Chemicals and antibodies

The following inhibitors/chemicals and antibodies were used in this study.

Cycloheximide (Enzo Life Sciences, 380-269-G005), PMA (EMD Millipore; 524400), Torin 1 (Tocris Bioscience; 4247), rapamycin (EMD Millipore; 553212), RSKi/BI-D1870 (Selleck Chemicals; S2843), MK-2206 (Selleck Chemicals; S1078), doxycycline (Fisher Bioreagents; BP26535), biotin phenol/biotinyl tyramide (Adipogen; CDX-B0270), and biotin (Sigma; B4639).

Monoclonal anti-HA-agarose mouse (Sigma; A2095), streptavidin agarose resin (Pierce; 20347), anti-FLAG M2 mouse (Sigma; F3165), streptavidin horseradish peroxidase (HRP) (Cell Signaling Technologies [CST]; 3999), pERK1/2 (CST; 4370), pRSK1 (CST; 9341), RSK1 (CST; 8408), RSK1/2/3 (CST; 14813, pAKT1 (CST; 4060), pS6K (CST; 9234), pS6 (CST; 8585), p4EBP1 (CST; 2855), myc (CST: 2278), tubulin (CST; 3873), TSC2 (Santa Crux; sc271314), pTSC2 (Santa Cruz; sc293149), HA (BioLegend; MMS-101P), Ltn1/RNF160 (Abcam; ab104375), RPS3 (Bethyl; A303-840A), RPL7 (Bethyl; A300-741A), and TTLL1 (Thermo Fisher; PA5-27285).

Knockdown studies

siRNA oligos were transfected into cells using RNAiMax (Thermo Fisher) according to the manufacturer guidelines at a final concentration of 10 nM. Oligos were purchased from Dharmacon (GE Lifesciences).

siRNA sequence

LTN1 #1 GCAGUGGUGUGAAGAAUUA

LTN1 #2 GAGAGUACCUUCCUACAUU

LTN1 #3 GCACUUACCUCACCCAUCA

NEMF #1 GGGAAGAGACAUUAAAUUA

NEMF #2 GAAGAAGACCGUGAACUUA

NEMF #3 GGACGAACCUGUGAAGAAA

Cell line generation and proximity labeling

293T and HCT116 cells were obtained from the American Type Culture Collection. Codon regions for the proteins of interest were recombined into FRT-tetO-FLAG-HA, BirA*-FLAG, or FLAG-APEX2 destination vectors using Gateway (Thermo Fisher) cloning methods. 293 Flp-In T-REx cell lines (Thermo Fisher catalogue number R78007) were transfected with Flp recombinase vector (pOG44) and FRT-tetO-expression vectors, and stable cell lines were selected with hygromycin. Cells were cultured in DMEM (High Glucose; Thermo Fisher catalogue #11995073) supplemented with 10% fetal bovine serum and penicillin/streptomycin. Protein expression was induced by adding 1 µg/ml doxycycline to the growth media for 16–20 h prior to cell harvesting. For cell lines expressing BirA*-tagged proteins, 50 µM biotin and 1 µg/ml doxycycline was added to the growth media for 16–20 h prior to cell harvesting. For cell lines expressing APEX2-tagged proteins, after 16 h dox treatment, cells were treated with 500 µM biotin-phenol (AdipoGen) for 1 h followed

by a 1-min treatment of 1.5 mM hydrogen peroxide. The reaction was quenched by addition of cold phosphate-buffered saline (PBS) with 5 mM Trolox and 10 mM sodium ascorbate to the cells.

Sucrose density gradient analysis

Cell lysis for sucrose gradient analysis was performed using digitonin lysis buffer (25 mM HEPES, pH 7.4, 125 mM KAc, 15 mM $MgAc_2$, 100 µg/ml digitonin, supplemented with 40U/ml RNase inhibitor, 50 µg/ml CHX, 1 mM dithiothreitol, and protease inhibitors). Protein (1.5 mg) was loaded onto a linear 5–45% sucrose gradient prepared using a gradient master (Biocomp). Ultracentrifugation was performed using a Beckman Coulter SW41 rotor at 35,000 rpm for 2.5 h. Fractions (1 ml) were collected manually starting from the top of the gradient. Fractions were then mixed with trichloroacetic acid (TCA) at a final concentration of 20%. Protein precipitates were washed once with 10% TCA, followed by three washes with 100% cold acetone. Protein precipitates were resuspended in 1× Laemmli sample buffer.

Sample processing for proteomics

Frozen cell pellets were lysed in mammalian cell lysis buffer (0.5% NP-40, 150 mM NaCl, 50 mM Tris, pH 7.8, protease inhibitors, 10 mM *N*-ethylmaleimide) at 4°C at an approximate 2:1 (vol:vol) ratio per pellet. Lysates were sonicated and clarified by centrifugation. Total protein was quantified using a bicinchoninic acid (BCA) protein assay (Pierce). For either FLAG or HA immunoprecipitation, cell lysates were mixed with 80 µl (1:1 slurry) of αHA-conjugated or αFLAG-conjugated agarose beads and incubated at 4°C overnight with constant rotation. For APEX2 and BioID samples, lysates were mixed with 80 µl (1:1 slurry) of streptavidin-conjugated agarose beads. After overnight incubations, the resin was washed 3× in wash buffer (0.1% NP-40, 150 mM NaCl, 50 mM Tris, pH 7.8, protease inhibitors) followed by three washes in cold PBS. For HA-IPs, proteins were eluted by addition of purified HA peptide (250 µg/ml). Proteins were precipitated from the eluate using a final concentration of 20% TCA. Protein precipitates were washed once with 10% TCA, followed by three washes with 100% cold acetone. Dried precipitates were digested with trypsin overnight at 37°C. (sequencing grade, Promega). For FLAG-IPs and streptavidin pull downs, trypsin was added to the washed resin and incubated overnight. Trypsin digested samples were desalted using the C18 stage-tip method.

Mass spectrometry

Eluted peptides were analyzed by liquid chromatography–mass spectrometry using a Q-Exactive (Thermo Fisher) and a nanoLC-easy 1000 (Thermo Fisher) essentially as described (Gendron *et al.*, 2016). A 1-h method with a 5–45% acetonitrile gradient was used. Data were processed and searched using the SEQUEST algorithm as described (Gendron *et al.*, 2016). For SILAC-based mapping of p97/VCP interacting proteins, proteins were considered as p97/VCP interacting proteins if the average Log2 SILAC ratio (H:L) between replicate experiments was less than –1, and the protein was quantified in at least two replicate experiments. For label-free proteomics, the D-score for all interacting proteins for both GFP and Ltn1 was calculated using CompPASS scoring (Sowa *et al.*, 2009). The D-score was normalized to the average D-score for all interacting proteins (both GFP and Ltn1) across all six conditions. Proteins were assigned as high confidence Ltn1 interacting proteins if the difference in the normalized D-score between GFP and Ltn1 (i.e., FH-Ltn1 D-score – FH-GFP D-score) was greater than 2. Mass spectrometry RAW files have been deposited at MassIVE and can be accessed with the accession number MSV000082006.

ACKNOWLEDGMENTS

We thank Brian Raught (University of Toronto) for providing BirA*-tagging expression plasmids. This work was supported by a New Scholar award from the Ellison Medical Foundation (E.J.B.), a Hellman Fellowship (E.J.B.), and the National Institutes of Health (DP2-GM119132) (E.J.B.). N.Z. is supported by the UCSD Cell and Molecular Genetics Training Program (T32 GM007240).

REFERENCES

Arakawa S, Yunoki K, Izawa T, Tamura Y, Nishikawa S, Endo T (2016). Quality control of nonstop membrane proteins at the ER membrane and in the cytosol. Sci Rep 6, 30795.

Bengtson MH, Joazeiro CA (2010). Role of a ribosome-associated E3 ubiquitin ligase in protein quality control. Nature 467, 470–473.

Bersuker K, Peterson CWH, To M, Sahl SJ, Savikhin V, Grossman EA, Nomura DK, Olzmann JA (2018). A proximity labeling strategy provides insights into the composition and dynamics of lipid droplet proteomes. Dev Cell 44, 97–112 e117.

Brandman O, Hegde RS (2016). Ribosome-associated protein quality control. Nat Struct Mol Biol 23, 7–15.

Brandman O, Stewart-Ornstein J, Wong D, Larson A, Williams CC, Li GW, Zhou S, King D, Shen PS, Weibezahn J, *et al.* (2012). A ribosome-bound quality control complex triggers degradation of nascent peptides and signals translation stress. Cell 151, 1042–1054.

Chen CL, Hu Y, Udeshi ND, Lau TY, Wirtz-Peitz F, He L, Ting AY, Carr SA, Perrimon N (2015). Proteomic mapping in live Drosophila tissues using an engineered ascorbate peroxidase. Proc Natl Acad Sci USA 112, 12093–12098.

Choe YJ, Park SH, Hassemer T, Korner R, Vincenz-Donnelly L, Hayer-Hartl M, Hartl FU (2016). Failure of RQC machinery causes protein aggregation and proteotoxic stress. Nature 531, 191–195.

Chu J, Hong NA, Masuda CA, Jenkins BV, Nelms KA, Goodnow CC, Glynne RJ, Wu H, Masliah E, Joazeiro CA, *et al.* (2009). A mouse forward genetics screen identifies LISTERIN as an E3 ubiquitin ligase involved in neurodegeneration. Proc Natl Acad Sci USA 106, 2097–2103.

Coyaud E, Mis M, Laurent EM, Dunham WH, Couzens AL, Robitaille M, Gingras AC, Angers S, Raught B (2015). BioID-based identification of Skp Cullin F-box (SCF)beta-TrCP1/2 E3 ligase substrates. Mol Cell Proteomics 14, 1781–1795.

Crowder JJ, Geigges M, Gibson RT, Fults ES, Buchanan BW, Sachs N, Schink A, Kreft SG, Rubenstein EM (2015). Rkr1/Ltn1 ubiquitin ligase-mediated degradation of translationally stalled endoplasmic reticulum proteins. J Biol Chem 290, 18454–18466.

Defenouillere Q, Yao Y, Mouaikel J, Namane A, Galopier A, Decourty L, Doyen A, Malabat C, Saveanu C, Jacquier A, *et al.* (2013). Cdc48-associated complex bound to 60S particles is required for the clearance of aberrant translation products. Proc Natl Acad Sci USA 110, 5046–5051.

Doamekpor SK, Lee JW, Hepowit NL, Wu C, Charenton C, Leonard M, Bengtson MH, Rajashankar KR, Sachs MS, Lima CD, *et al.* (2016). Structure and function of the yeast listerin (Ltn1) conserved N-terminal domain in binding to stalled 60S ribosomal subunits. Proc Natl Acad Sci USA 113, E4151–E4160.

Drummond DA, Wilke CO (2009). The evolutionary consequences of erroneous protein synthesis. Nat Rev Genet 10, 715–724.

Garzia A, Jafarnejad SM, Meyer C, Chapat C, Gogakos T, Morozov P, Amiri M, Shapiro M, Molina H, Tuschl T, *et al.* (2017). The E3 ubiquitin ligase and RNA-binding protein ZNF598 orchestrates ribosome quality control of premature polyadenylated mRNAs. Nat Commun 8, 16056.

Gendron JM, Webb K, Yang B, Rising L, Zuzow N, Bennett EJ (2016). Using the ubiquitin-modified proteome to monitor distinct and spatially restricted protein homeostasis dysfunction. Mol Cell Proteomics 15, 2576–2593.

Harper JW, Bennett EJ (2016). Proteome complexity and the forces that drive proteome imbalance. Nature 537, 328–338.

Hesketh GG, Youn JY, Samavarchi-Tehrani P, Raught B, Gingras AC (2017). Parallel exploration of interaction space by BioID and affinity purification coupled to mass spectrometry. Methods Mol Biol 1550, 115–136.

Higgins R, Gendron JM, Rising L, Mak R, Webb K, Kaiser SE, Zuzow N, Riviere P, Yang B, Fenech E, *et al.* (2015). The unfolded protein response triggers site-specific regulatory ubiquitylation of 40S ribosomal proteins. Mol Cell 59, 35–49.

Hung V, Lam SS, Udeshi ND, Svinkina T, Guzman G, Mootha VK, Carr SA, Ting AY (2017). Proteomic mapping of cytosol-facing outer mitochondrial and ER membranes in living human cells by proximity biotinylation. Elife 6, e24463.

Hung V, Udeshi ND, Lam SS, Loh KH, Cox KJ, Pedram K, Carr SA, Ting AY (2016). Spatially resolved proteomic mapping in living cells with the engineered peroxidase APEX2. Nat Protoc 11, 456–475.
Iconomou M, Saunders DN (2016). Systematic approaches to identify E3 ligase substrates. Biochem J 473, 4083–4101.
Ishimura R, Nagy G, Dotu I, Zhou H, Yang XL, Schimmel P, Senju S, Nishimura Y, Chuang JH, Ackerman SL (2014). RNA function. Ribosome stalling induced by mutation of a CNS-specific tRNA causes neurodegeneration. Science 345, 455–459.
Izawa T, Park SH, Zhao L, Hartl FU, Neupert W (2017). Cytosolic protein Vms1 links ribosome quality control to mitochondrial and cellular homeostasis. Cell 171, 890–903 e818.
Joazeiro CAP (2017). Ribosomal stalling during translation: providing substrates for ribosome-associated protein quality control. Annu Rev Cell Dev Biol 33, 343–368.
Juszkiewicz S, Hegde RS (2017). Initiation of quality control during poly(A) pranslation requires site-specific ribosome ubiquitination. Mol Cell 65, 743–750 e744.
Kim DI, Roux KJ (2016). Filling the void: proximity-based labeling of proteins in living cells. Trends Cell Biol 26, 804–817.
Kostova KK, Hickey KL, Osuna BA, Hussmann JA, Frost A, Weinberg DE, Weissman JS (2017). CAT-tailing as a fail-safe mechanism for efficient degradation of stalled nascent polypeptides. Science 357, 414–417.
Lam SS, Martell JD, Kamer KJ, Deerinck TJ, Ellisman MH, Mootha VK, Ting AY (2015). Directed evolution of APEX2 for electron microscopy and proximity labeling. Nat Methods 12, 51–54.
Lara R, Seckl MJ, Pardo OE (2013). The p90 RSK family members: common functions and isoform specificity. Cancer Res 73, 5301–5308.
Lee JW, Beebe K, Nangle LA, Jang J, Longo-Guess CM, Cook SA, Davisson MT, Sundberg JP, Schimmel P, Ackerman SL (2006). Editing-defective tRNA synthetase causes protein misfolding and neurodegeneration. Nature 443, 50–55.
Lobingier BT, Huttenhain R, Eichel K, Miller KB, Ting AY, von Zastrow M, Krogan NJ (2017). An approach to spatiotemporally resolve protein interaction networks in living cells. Cell 169, 350–360 e312.
Loh KH, Stawski PS, Draycott AS, Udeshi ND, Lehrman EK, Wilton DK, Svinkina T, Deerinck TJ, Ellisman MH, Stevens B, *et al*. (2016). Proteomic analysis of unbounded cellular compartments: synaptic clefts. Cell 166, 1295–1307 e1221.
Lykke-Andersen J, Bennett EJ (2014). Protecting the proteome: eukaryotic cotranslational quality control pathways. J Cell Biol 204, 467–476.
Lyumkis D, Oliveira dos Passos D, Tahara EB, Webb K, Bennett EJ, Vinterbo S, Potter CS, Carragher B, Joazeiro CA (2014). Structural basis for translational surveillance by the large ribosomal subunit-associated protein quality control complex. Proc Natl Acad Sci USA 111, 15981–15986.
Markmiller S, Soltanieh S, Server KL, Mak R, Jin W, Fang MY, Luo EC, Krach F, Yang D, Sen A, *et al*. (2018). Context-dependent and disease-specific diversity in protein interactions within stress granules. Cell 172, 590–604 e513.
Matsuda R, Ikeuchi K, Nomura S, Inada T (2014). Protein quality control systems associated with no-go and nonstop mRNA surveillance in yeast. Genes Cells 19, 1–12.
Matsuo Y, Ikeuchi K, Saeki Y, Iwasaki S, Schmidt C, Udagawa T, Sato F, Tsuchiya H, Becker T, Tanaka K, *et al*. (2017). Ubiquitination of stalled ribosome triggers ribosome-associated quality control. Nat Commun 8, 159.
Maurer MJ, Spear ED, Yu AT, Lee EJ, Shahzad S, Michaelis S (2016). Degradation signals for ubiquitin-proteasome dependent cytosolic protein quality control (CytoQC) in yeast. G3 (Bethesda) 6, 1853–1866.
Noma A, Kirino Y, Ikeuchi Y, Suzuki T (2006). Biosynthesis of wybutosine, a hyper-modified nucleoside in eukaryotic phenylalanine tRNA. EMBO J 25, 2142–2154.
O'Connor HF, Huibregtse JM (2017). Enzyme-substrate relationships in the ubiquitin system: approaches for identifying substrates of ubiquitin ligases. Cell Mol Life Sci 74, 3363–3375.
Perche-Letuvee P, Molle T, Forouhar F, Mulliez E, Atta M (2014). Wybutosine biosynthesis: structural and mechanistic overview. RNA Biol 11, 1508–1518.
Pisareva VP, Skabkin MA, Hellen CU, Pestova TV, Pisarev AV, (2011). Dissociation by Pelota, Hbs1 and ABCE1 of mammalian vacant 80S ribosomes and stalled elongation complexes. EMBO J 30, 1804–1817.
Reinke AW, Balla KM, Bennett EJ, Troemel ER (2017a). Identification of microsporidia host-exposed proteins reveals a repertoire of rapidly evolving proteins. Nat Commun 8, 14023.
Reinke AW, Mak R, Troemel ER, Bennett EJ (2017b). In vivo mapping of tissue- and subcellular-specific proteomes in Caenorhabditis elegans. Sci Adv 3, e1602426.
Rhee HW, Zou P, Udeshi ND, Martell JD, Mootha VK, Carr SA, Ting AY (2013). Proteomic mapping of mitochondria in living cells via spatially restricted enzymatic tagging. Science 339, 1328–1331.
Romeo Y, Zhang X, Roux PP (2012). Regulation and function of the RSK family of protein kinases. Biochem J 441, 553–569.
Roux KJ, Kim DI, Raida M, Burke B (2012). A promiscuous biotin ligase fusion protein identifies proximal and interacting proteins in mammalian cells. J Cell Biol 196, 801–810.
Roux PP, Ballif BA, Anjum R, Gygi SP, Blenis J (2004). Tumor-promoting phorbol esters and activated Ras inactivate the tuberous sclerosis tumor suppressor complex via p90 ribosomal S6 kinase. Proc Natl Acad Sci USA 101, 13489–13494.
Sapkota GP, Cummings L, Newell FS, Armstrong C, Bain J, Frodin M, Grauert M, Hoffmann M, Schnapp G, Steegmaier M, *et al*. (2007). BI-D1870 is a specific inhibitor of the p90 RSK (ribosomal S6 kinase) isoforms in vitro and in vivo. Biochem J 401, 29–38.
Shao S, Brown A, Santhanam B, Hegde RS (2015). Structure and assembly pathway of the ribosome quality control complex. Mol Cell 57, 433–444.
Shao S, Hegde RS (2014). Reconstitution of a minimal ribosome-associated ubiquitination pathway with purified factors. Mol Cell 55, 880–890.
Shao S, von der Malsburg K, Hegde RS (2013). Listerin-dependent nascent protein ubiquitination relies on ribosome subunit dissociation. Mol Cell 50, 637–648.
Shcherbik N, Chernova TA, Chernoff YO, Pestov DG (2016). Distinct types of translation termination generate substrates for ribosome-associated quality control. Nucleic Acids Res 44, 6840–6852.
Shen PS, Park J, Qin Y, Li X, Parsawar K, Larson MH, Cox J, Cheng Y, Lambowitz AM, Weissman JS, *et al*. (2015). Protein synthesis. Rqc2p and 60S ribosomal subunits mediate mRNA-independent elongation of nascent chains. Science 347, 75–78.
Shoemaker CJ, Eyler DE, Green R (2010). Dom34:Hbs1 promotes subunit dissociation and peptidyl-tRNA drop-off to initiate no-go decay. Science 330, 369–372.
Shoemaker CJ, Green R (2012). Translation drives mRNA quality control. Nat Struct Mol Biol 19, 594–601.
Sowa ME, Bennett EJ, Gygi SP, Harper JW (2009). Defining the human deubiquitinating enzyme interaction landscape. Cell 138, 389–403.
Sundaramoorthy E, Leonard M, Mak R, Liao J, Fulzele A, Bennett EJ (2017). ZNF598 and RACK1 regulate mammalian ribosome-associated quality control function by mediating regulatory 40S ribosomal ubiquitylation. Mol Cell 65, 751–760e754.
Tsuboi T, Kuroha K, Kudo K, Makino S, Inoue E, Kashima I, Inada T (2012). Dom34:hbs1 plays a general role in quality-control systems by dissociation of a stalled ribosome at the 3′ end of aberrant mRNA. Mol Cell 46, 518–529.
Verma R, Oania RS, Kolawa NJ, Deshaies RJ (2013). Cdc48/p97 promotes degradation of aberrant nascent polypeptides bound to the ribosome. Elife 2, e00308.
von der Malsburg K, Shao S, Hegde RS (2015). The ribosome quality control pathway can access nascent polypeptides stalled at the Sec61 translocon. Mol Biol Cell 26, 2168–2180.
Wisniewski JR, Hein MY, Cox J, Mann M (2014). "A "proteomic ruler" for protein copy number and concentration estimation without spike-in standards." Mol Cell Proteomics 13, 3497–3506.
Xue L, Blythe EE, Freiberger EC, Mamrosh JL, Hebert AS, Reitsma JM, Hess S, Coon JJ, Deshaies RJ (2016). Valosin-containing protein (VCP)-adaptor interactions are exceptionally dynamic and subject to differential modulation by a VCP inhibitor. Mol Cell Proteomics 15, 2970–2986.
Yonashiro R, Tahara EB, Bengtson MH, Khokhrina M, Lorenz H, Chen KC, Kigoshi-Tansho Y, Savas JN, Yates JR, Kay SA, *et al*. (2016). The Rqc2/Tae2 subunit of the ribosome-associated quality control (RQC) complex marks ribosome-stalled nascent polypeptide chains for aggregation. Elife 5, e11794.